LoRa Technology Demystified: From Link Behavior to Cell-Level Performance

Daniele Croce, Michele Gucciardo, Stefano Mangione, Giuseppe Santaromita, and Ilenia Tinnirello

***Abstract*— In this paper we study the capability of LoRa technology in rejecting different interfering LoRa signals and the impact on the cell capacity. First, we analyze experimentally the link-level performance of LoRa and show that collisions between packets modulated with the same Spreading Factor (SF) usually lead to channel captures, while different spreading factors can indeed cause packet loss if the interference power is strong enough. Second, we model the effect of such findings to quantify the achievable capacity in a typical LoRa cell: we show that high SFs, generally seen as more robust, can be severely affected by inter-SF interference and that different criteria for deciding SF allocations within the cell may lead to significantly different results. Moreover, the use of power control and packet fragmentation can be detrimental more than beneficial in many deployment scenarios. Finally, we discuss the capacity improvements that can be achieved by increasing the density of LoRa gateways. Our results have important implications for the design of LoRa networks: for example, allocating high SFs to faraway end devices might not improve the experienced performance in case of congested networks because of the increased transmission time and vulnerability period.**

***Index Terms*— LoRa, spreading factor, interference.**

I. Introduction

IN RECENT years, we have assisted to an impressive proliferation of wireless technologies and mobile-generated traffic, which is now the highest portion of the total internet traffic [1]. Such proliferation has been characterized by high-density deployments of base stations (based on heterogeneous technologies, such as 4G cellular base stations and WiFi Access Points), and a pervasive diffusion of wireless devices, not limited to traditional user terminals. Indeed, with the advent of Internet-of-Things (IoT) applications, many smart objects, such as domestic appliances, cameras, monitoring sensors, etc., are equipped with a wireless technology.

In this paper we consider the emerging Long Range (LoRa) technology, which represents a critical example of wireless technology working in high-density scenarios. Indeed, LoRa has been conceived for Low Power Wide Area Networks (LPWANs), characterized by low data rate requirements per single device, large cells and heterogeneous application domains, which may lead to extremely high numbers of end devices (EDs) coexisting in the same cell. For this reason, LoRa provides different possibilities to orthogonalize transmissions as much as possible – Carrier Frequency (CF), Spreading Factor (SF), Bandwidth (BW), Coding Rate (CR) – and provides simultaneous collision free communications. However, despite the robustness of the LoRa PHY [2] patented by Semtech, in WAN scenarios where multiple gateways can be installed, the scalability of this technology is still under investigation [3]. Current studies are mostly based on the assumption that using multiple transmission channels and spreading factors leads to a system that can be considered as the simple super-position of independent (single channel, single SF) sub-systems [4]. This is actually a strong simplification, especially because the SFs adopted by LoRa are pseudo-orthogonal [5] and therefore, in near-far conditions, collisions can prevent the correct reception of the overlapping transmissions using different SFs.

For characterizing these phenomena, in this paper we provide two main contributions: a link-level characterization of LoRa modulation (based on our previous work [6]) and then, exploiting such link-level properties, we provide a complete cell model study of multi-link LoRa systems. Regarding the first aspect, we characterize LoRa modulation experimentally, showing that collisions between packets of different SFs can indeed cause packet loss. We modified the software transceiver presented in [7] to generate synthesized LoRa modulated packets and transmit them through the well-known USRP software-defined-radio (SDR) platform. This transceiver is used to emulate, in a controlled and repeatable manner, collisions produced by different devices: the modulated LoRa signals are first generated in software, then summed together (with tunable power level difference) to replicate a given super-position of LoRa signals and finally the obtained combined radio signal is transmitted over the air. We use this traffic generator to experimentally characterize the performance of a commercial LoRa device, under intra-SF and inter-SF collisions caused by multiple simultaneously active LoRa links. We quantify the power difference for which capture effects and packet loss occur, for all combinations of SFs. Our experimental results show that the co-channel rejection thresholds are on average an order of magnitude higher than the theoretical ones presented in [8], with values as high as -8 dB. These poor co-channel rejection thresholds might be insufficient in common LoRa application scenarios (the received power

Manuscript received October 22, 2018; revised April 29, 2019; accepted October 7, 2019. Date of publication October 29, 2019; date of current version February 11, 2020. The associate editor coordinating the review of this article and approving it for publication was R. Hu. *(Corresponding author: Daniele Croce.)*

The authors are with the Engineering Department, Università di Palermo, 90133 Palermo, Italy, and also with the CNIT Consortium, 43100 Parma, Italy (e-mail: daniele.croce@unipa.it).

Color versions of one or more of the figures in this article are available online at http://ieeexplore.ieee.org.

Digital Object Identifier 10.1109/TWC.2019.2948872

of two radio signals can easily differ by tens of dB), thus contradicting the common belief that pseudo-orthogonal SFs can be considered as orthogonal in practice.

The second main contribution of the paper regards the capacity analysis of a LoRa cell under realistic link behaviors: we propose a simple yet accurate analytical framework to model the performance of LoRa cells, deriving the aggregated capacity and data extraction rate of a LoRa cell working on a single frequency with one or multiple gateways. The framework has been built as a generalization of the Aloha model (the channel access protocol used in LoRa), by taking into account the heterogeneous probabilities of intra-SF and inter-SF collisions, due to the specific position of the target ED (which translates in a specific received power at the gateway). The models provide excellent results, closely following the simulations obtained with LoRaSim [9] and with our own custom Matlab simulator. Our analysis demonstrates that capture effects and imperfect orthogonality of SFs can significantly affect the cell capacity. In particular, we show that more robust SFs, usually envisioned for EDs experiencing strong channel attenuations, can be severely affected by inter-SF interference and therefore, their usage could consume a large fraction of cell resources without real benefits. Also, we show that power control and packet fragmentation can be counterproductive. Finally, we quantify the performance increase obtained by deploying multiple gateways and we show that it might be best to deploy them at the edge of the cell more than on a regular grid.

The rest of the paper is organized as follows. After a brief review of literature work about LoRa performance evaluation in §II, we provide a background description of LoRa modulation and a characterization of link-level performance in §III. The analysis of cell capacity is presented in §IV, while in §V we extend our model in case of non-uniform allocation of SFs, power control and packet fragmentation. Finally, we analyze the capacity improvements achievable with multiple gateways and the performance impact of topology in §VI and conclude our paper in §VII.

II. Related Work

A. LoRa Technology

Since LoRa is quite a recent technology, apart from general descriptions of LoRa applications [10] and implications for IoT scenarios, relatively few works have already been published on the evaluation of LoRa link-level performance or cell capacity. Link-level studies are mostly based on the experimental characterization of coverage and interference rejection capabilities of the LoRa PHY, patented by Semtech [11]. LoRa modulation is presented in [12], together with an implementation of a software LoRa transceiver, called *gr-lora*, based on Software-Defined-Radio. The paper in [8] quantifies the power reception thresholds for different modulation formats and the Signal-to-Interference-Ratio (SIR) required for rejecting interfering LoRa signals, modulated with different spreading factors. However, no justification about the derivation of these numbers is provided and, as we will show, their theoretical results are very different from our experimental ones. In [5] link-level performance of LoRa are compared with ultra narrowband (Sigfox-like) networks, concluding that ultra narrowband has a larger coverage but LoRa networks are less sensitive to interference.

Capacity results of LoRa cells are based on the characterization of link behaviors. In [3], the authors experimentally demonstrate the capture phenomena between colliding LoRa frames, and then use these results for quantifying the cell capacity in simulation [9], in terms of maximum number of devices that can be served with a desired data extraction rate. The simulator assumes that it is enough a power ratio of 6dB between colliding frames to correctly demodulate the one received at the highest power, and that multiple transmissions with different spreading factor can be considered as perfectly orthogonal [4]. This last assumption is a strong simplification, because the spreading factors adopted by LoRa are pseudo-orthogonal [5] and, as we will show, inter-SF collisions can indeed be an issue in near-far conditions, when the interferer is close to the receiver. Despite this simplification, in [3] the authors show that a typical deployment can support only 120 EDs per 3.8 ha, although performance can be improved by using multiple gateways (i.e. by increasing the probability of capture events). The cell capacity is compared with pure Aloha networks, while no model is provided for characterizing the impact of channel captures. In [13], authors use a LoRa cell performance model in a scenario with high number of devices and propose solutions to improve its performance, but no detail is provided about the model.

An important aspect affecting the cell capacity is the SF allocations within the cell. LoRa technology defines a default Adaptive Data Rate (ADR) scheme for deciding the SF to be used by each device, based on the selection of the minimum SF compatible with the available link budget. Such a choice guarantees that each device achieves the highest possible data rate with local decisions. Another approach proposed in [14] assigns the SFs by also considering load balancing between different SFs: this improves the cell capacity, although the authors ignore inter-SF interference. The work in [15] presents a SF allocation scheme which jointly works on SF and power allocation in a single cell scenario, for achieving the optimal device distribution presented in [16]. Also in this case, the scheme acts without considering the capture effect and by assuming orthogonal SFs. Finally, the use of multi-channel MAC protocols could be used to improve the cell performance, as proposed in [21]. The results presented in this paper are valid also in case multiple channels are used, for analyzing the performance of the single channels separately.

B. Capture Models

Capture effects can significantly boost the performance of random access schemes, because some collision events may result in the correct reception of the strongest signal. For modeling this phenomena, different approaches have been considered so far, based on evaluation of the interfering power, colliding times, channel fades, etc. The characterization of the interfering power, which in turns depends on the number

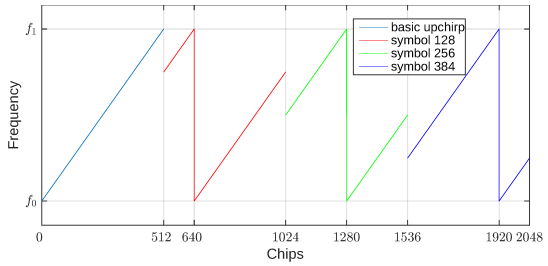

Fig. 1. Modulating signal with $SF = 9$ for one basic upchirp and three symbols: 128, 256 and 384.

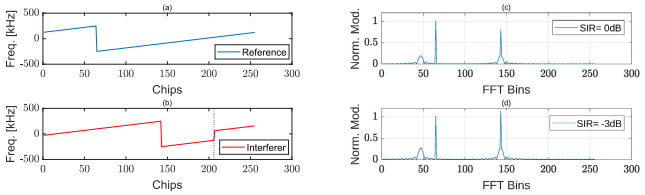

Fig. 2. An example of capture effect within signals modulated with same SF 8. A LoRa reference symbol (a) and two partially overlapping interfering symbols (b) are received at different SIR levels. The iFFT output after multiplication with the base SF 8 downchirp and downsampling shows the highest peak for the perfectly synchronized reference symbol and two lower peaks for the partially overlapping symbols (c) but a SIR of -3 dB is enough to overcome the reference signal (d).

of interfering signals, can be used for estimating channel captures when the SIR of a target frame is higher than a capture threshold [17]. Alternatively, it is possible to map the highest possible interference level into a vulnerability circle, out of which interfering signals do not affect packet reception [18]. Despite its simplicity, this approach leads to good results when the network works in stable conditions. Therefore, we chose to follow this approach, by generalizing the concept of vulnerability circle to both intra-SF and inter-SF interfering signals.

III. LoRa Link-Level Behavior

A. LoRa Modulation and Demodulation

LoRa modulation is derived from *Chirp Spread Spectrum (CSS)*, which makes use of *chirp signals*, i.e. frequency-modulated signals obtained when the modulating signal varies linearly in the range $[f_0, f_1]$ (upchirp) or $[f_1, f_0]$ (downchirp) in a symbol time T. Binary modulations, mapping 0/1 information bits in upchirps/downchirps, have been demonstrated to be very robust against in-band or out-band interference [2]. LoRa employs a M-ary modulation scheme based on chirps, in which symbols are obtained by considering different circular shifts of the basic upchirp signal. The temporal shifts, characterizing each symbol, are slotted into multiples of time $T_{chip} = 1/BW$, called chip, being $BW = f_1 - f_0$ the bandwidth of the signal. It results that the modulating signal for a generic n-th LoRa symbol can be expressed as:

$$f(t) = \begin{cases} f_1 + k(t - n \cdot T_{chip}) & \text{for } 0 \leqslant t \leqslant n \cdot T_{chip} \\ f_0 + k(t - n \cdot T_{chip}) & \text{for } n \cdot T_{chip} < t \leqslant T \end{cases}$$

where $k = (f_1 - f_0)/T$ is the slope of the frequency variations. The total number of symbols (coding i information bits) is chosen equal to 2^i, where i is called spreading factor. The symbol duration T required for representing any possible shift is $T = 2^i \cdot T_{chip} = 2^i/BW$. It follows that, for a fixed bandwidth, the symbol period and the temporal occupancy of the signal increase with larger SFs. Fig. 1 shows the modulating signal used for a basic upchirp and three examples of circular shifts obtained for a SF equal to 9: the symbol time is 512 T_{chip}, while the three exemplary shifts code the symbols 128, 256 and 384.

The preamble of any LoRa frame is obtained by sending a sequence of at least eight upchirps followed by two coded upchirps, used for network identification (sync word), and two and a quarter base downchirps. Payload data are then sent by using the M-ary modulation symbols. LoRa provides three BW settings (125, 250 or 500 kHz) and seven different SF values (from 6 to 12). In general, a larger bandwidth translates in a data rate increase and a receiver sensitivity deterioration. Conversely, higher spreading factors can be used for improving the link robustness at the cost of a lower data rate. For demodulation, the received LoRa signal is synchronously multiplied to the base downchirp. This results in a signal comprising only two frequencies: $f_n = -kn \cdot T_{chip}$ and $f_n - BW = -(f_1 - f_0) - kn \cdot T_{chip}$. Both frequencies will be aliased to the same frequency f_n by downsampling at the rate BW. The estimated symbol index $\hat{n}$ corresponds to the position of the peak at the output of an iFFT, as described in [8].

An interesting feature of LoRa modulation is the orthogonality of signals modulated under different spreading factors, which can be exploited for enabling multiple concurrent transmissions. Although perfect orthogonality is guaranteed only in case of exact synchronization of the transmitters, the cross-energy between two signals modulated with different spreading factors is almost zero, regardless of the starting of the symbol times. In case of collisions with other LoRa symbols, we can distinguish two different scenarios, depending on the interfering spreading factor SF_{int}. First, if the SF_{int} is the same as the one the receiver is listening for, the above receiver will observe multiple peaks at the output of the iFFT. Indeed, assuming that the two transmissions are received at the same power and that the reference signal is perfectly synchronized with the receiver, the iFFT will show a maximum peak corresponding to the reference symbol and two smaller peaks corresponding to two partially overlapping interference symbols, with different height depending on the transmitted symbols and on the offset with the receiver. For example, Fig. 2 shows two signals modulated with same SF 8 and bandwidth 500 kHz: the reference symbol (Fig. 2-a) and two partially overlapping interfering symbols (Fig. 2-b). As depicted in Fig. 2-c, when the signals are received with the same power, the iFFT output after multiplication with the base downchirp and downsampling, shows the highest peak for the synchronized reference symbol (index $\hat{n} = 64$) and two lower peaks for the partially overlapping symbols (index $\hat{n_1} = 96$ and $\hat{n_2} = 192$, with shift of $0.2T$ – i.e. 51.2).

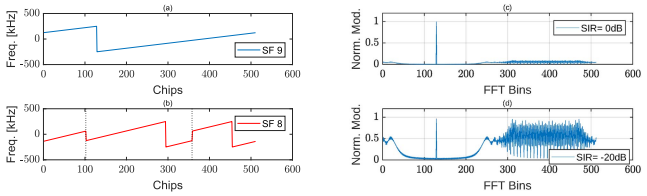

Fig. 3. An example of collision between signals modulated with different SF. A LoRa symbol modulated with SF equal to 9 (a) and two overlapping and circularly shifted interfering symbols with SF 8 (b) are simultaneously received at different SIR levels. The iFFT output after multiplication with the base SF 9 downchirp and downsampling shows a clear peak when the two signals have the same power (c) while this is not the case when the SIR is too low (d).

However, a Signal to Interference Ratio (SIR) of -3dB is enough for the interfering signal to overcome the reference signal and "capture" the channel (Fig. 2-d). This means that LoRa exhibits a very high capture probability within the same SF.

Second, when the SF_{int} is different from the one the receiver is interested in, after multiplication with the base downchirp and downsampling, the interfering signal will still be a chirped waveform, resulting in a wide-band spectrum with low spectral density. An example is illustrated in Fig. 3, where one signal modulated with SF equal to 9 (Fig. 3-a) is overlapped to two symbols modulated with SF 8 (Fig. 3-b), circularly shifted to de-synchronize them with the reference symbol (the dotted lines represent the boundaries of the symbols). At the receiver, when the two signals are received with same power, the iFFT output after multiplication with the base SF 9 downchirp and downsampling shows a clear peak corresponding to the reference SF 9 symbol index $\hat{n} = 128$ (Fig. 3-c), while this is not the case when the SIR is too low because of the non perfect SF orthogonality (Fig. 3-d). In this scenario, the co-channel rejection is much higher (≈ -20dB in the figure).

B. Co-Channel Rejection

To quantify the impact of collisions and measure the co-channel rejection, we performed a number of experiments on a real point-to-point LoRa link in presence of continuous collisions of packets. Our goal is identifying a SIR threshold under which the demodulation of the received frame is affected by errors. In particular, to characterize the behavior of a commercial LoRa receiver in presence of inter-SF and intra-SF collisions, we used a Semtech SX1272 transceiver, controlled by an Arduino Yun. We modified the LoRa synthesizer presented in [7] to encode, modulate and generate the I/Q samples of a real LoRa packet, which are then transmitted over the air with a USRP B210 board through GNU radio. With this LoRa synthesizer, we generated two traces (one for the interferer and one for the reference LoRa link) for each combination of spreading factors, composed of a stream of 500 packets with a 20 byte payload (for the reference SF_{ref}) and adjusting the payload length of the interfering SF_{int} to match the length of the reference trace, i.e. with an equivalent time on air. The offset of each interfering packet, overlapped in time to the packets of the reference link, has been randomly selected within a window which guarantees that the two packets collide for at least one symbol. We filled the payload of the frames with randomly generated bytes, except for the two bytes that specify the destination address and the payload length. In particular, we assigned the destination address of the SX1272 receiver only to the packets of the reference link. This allows the receiver to discard the interfering packets when they are modulated with the same spreading factor of the reference ones (i.e. $SF_{int} = SF_{ref}$). Finally, we scaled the amplitude of the interfering packet stream to achieve the desired SIR, varying from -30 dB to $+6$ dB, and added it to the reference stream. The resulting combined stream, which emulates the traffic generated by two different transmitters, was transmitted through the USRP towards the receiving SX1272 module. The experiments were performed in our lab, with the transmitter and receiver about 1 meter apart using omnidirectional half wave antennas.

TABLE I
SIR THRESHOLDS IN dB WITH SX1272 TRANSCEIVER

SF_{ref} \ SF_{int}	7	8	9	10	11	12
7	1	-8	-9	-9	-9	-9
8	-11	1	-11	-12	-13	-13
9	-15	-13	1	-13	-14	-15
10	-19	-18	-17	1	-17	-18
11	-22	-22	-21	-20	1	-20
12	-25	-25	-25	-24	-23	1

The results of the experiments are summarized in table I, for all spreading factor combinations. The table shows that LoRa co-channel rejection is almost independent of the interfering SF and on average is around -16dB, about 10dB – an order of magnitude – higher than the theoretical results of [8], with values as high as -8 dB. Note that the results of [8] have not been justified in the paper and are quite different from our experimental ones.[1] This contradicts the common belief that SFs can be considered orthogonal, because in typical near-far conditions, when the interferer is much closer to the LoRa receiver, inter-SF collisions can indeed be an issue.

IV. ANALYSIS OF SINGLE CELL CAPACITY

The brief description of the LoRa PHY presented in section III enlightens two important aspects that have to be considered for studying the real capacity of LoRa cells: i) the possibility of correctly receiving a packet, in case of collision with other packets modulated with the same SF; ii) the possibility that multiple SFs are not exactly orthogonal and therefore do not work as independent multiple channels. In this section we show that both these aspects have a strong effect on the uplink cell capacity, because of the simple access scheme used in LoRa, which is basically a non-slotted Aloha mechanism (without carrier sense). We derive some simple expressions for predicting LoRa uplink capacity in presence of a single gateway, in terms of average throughput,

[1]The values presented in Table I of [8] follow $-10\ log_{10}(2^{SF_{ref}})$ in the lower triangular part, while on the upper triangular part are similar to $-10\ log_{10}(2^{SF_{ref}}) + 10\ log_{10}((2^{SF_{int}} - 2^{SF_{ref}})/(2^{SF_{int}} + 2^{SF_{ref}}))$. However, these results do not reflect the actual behavior of LoRa, as demonstrated in [6].

TABLE II
SIMULATION PARAMETERS

Parameter	Value
Carrier Frequency	868.0 MHz
Transmission Power	14 dBm
Bandwidth	500 kHz
Code Rate	4/5
Message size	20 Bytes
Message Period	90000 ms
Number of EDs	[50-2000]
Path loss attenuation exponent	4
Simulation time	9000 s

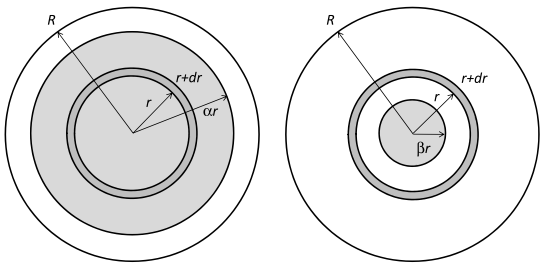

Fig. 4. Traffic competing with receivers placed in the circular ring between r and $r+dr$ (dark gray area): distribution of intra-SF (left cell) and inter-SF (right cell) competing load.

by generalizing the classical Aloha results in presence of channel captures and imperfect orthogonality between SFs. We also compare our capacity models with simulation results obtained by using a custom Matlab simulator, which we also validated against the LoRaSim simulator [9] used by the authors of [3] (which we warmly thank for publishing the source code). Unless specified otherwise, the parameters used for configuring the reference LoRa cell are summarized in table II.

A. LoRa Cell Capacity With Ideal Links

LoRa cells work as non-slotted Aloha systems. Under Poisson packet arrivals, the throughput of an ideal non-slotted Aloha cell is $G \cdot e^{-2G}$, being G the normalized load offered in the cell, i.e. the amount of data transmitted in the unit time by the EDs over nominal channel capacity. The Data Extraction Rate (DER), i.e. the probability of correctly receiving a packet transmission – a typical parameter for characterizing LoRa systems–, is given by e^{-2G}. In ideal conditions, since different SFs are available, the system works as the super-position of multiple coexisting (but independent) Aloha systems, each one experiencing the load due to the EDs employing a given SF equal to i (with $i \in \{7, 12\}$).

Let $G_i = \lambda_i \cdot ToA_i$ be the load offered in the cell sub-system working with SF i, which depends on the packet arrival rate λ_i and packet transmission time ToA_i (also called Time on Air or airtime). The ToA_i values change significantly from one SF to another. Indeed, the time interval required for transmitting a packet is given by the sum of the preamble time, which lasts n_{ph} symbol times T, and the payload transmission time. Since each symbol codes i bits and a channel coding with rate $CR = 4/(4 + RDD)$ is applied (with redundancy bits $RDD = 1, \ldots, 4$), the time ToA_i required for transmitting a frame long P bytes with SF i can be expressed as $(n_{ph} + \lceil \frac{P \cdot 8}{i \cdot 4} \rceil \cdot (4 + RDD)) \cdot T$. Thus, the total uplink capacity results equal to $\sum_{i=7}^{12} G_i e^{-2\ G_i}$ and can be dramatically reduced (down to zero) as the loads G_i increase (up to infinity).

Obviously, in a real cell the number n_i of EDs working on a given SF i is generally high but finite, and λ_i can be evaluated as $n_i \cdot s$, being s the source rate of each ED (which we assume to be constant for all devices). In absence of capture effects and inter-SF interference, the cell capacity is affected solely by the number of EDs configured on each SF, but it does not depend on the spatial distribution of the EDs within the cell (provided that all EDs are in the coverage range of the gateway).

B. Impact of Channel Captures

Consider first the case when collisions are only due to frames using the same SF (i.e. different SFs are perfectly orthogonal) and the spatial distribution of the devices is uniform in the whole cell area. As discussed in §III, LoRa modulation is very robust to interfering signals, and therefore it is very likely that the frames colliding at a given gateway result in the correct reception of the strongest one. For quantifying the performance improvements due to these events, we assume that in most practical cases a target ED can be interfered by a single colliding signal at a time. As we will show, this assumption is reasonable when the cell works in stable, non-congested conditions.

Capture effects have been observed when the reception power of the colliding signal is sufficiently lower than the power of the target ED (i.e. the SIR of the target ED in dB is higher than a positive threshold, which we experimentally found equal to 1 dB, as shown in table I). For a transmitter located at distance r from the gateway, neglecting the effect of random fading and assuming uniform transmission power among EDs and an attenuation law of type $r^{-\eta}$, this capture condition can be mapped into the placement of the interfering ED in a circular ring delimited by a distance αr, with $\alpha = 10^{SIR/10\eta} > 1$, and the cell radius R. An exemplary representation of this area in which the interfering ED does not prevent the reception of the target ED is shown in the left-most cell of Fig. 4 in white. Obviously, when αr is higher than R, such a region does not exist, because the transmitter is too far from the gateway and captures cannot occur. It follows that a target ED employing a given SF i is actually competing with a fraction of the total load G_i, which corresponds to the ratio between the area of the circle of radius $\min(\alpha r, R)$ and the total area of the cell. The smaller the α coefficient, the smaller the real competing load is. Note that in case of severe attenuation, higher values of η translate to lower values of α and higher chances of channel captures. Without loss of generality, in our numerical experiments we use $\eta = 4$.

To model the performance of LoRa in presence of channel captures, we extend the basic non-slotted Aloha model exploiting the above considerations: assuming for simplicity

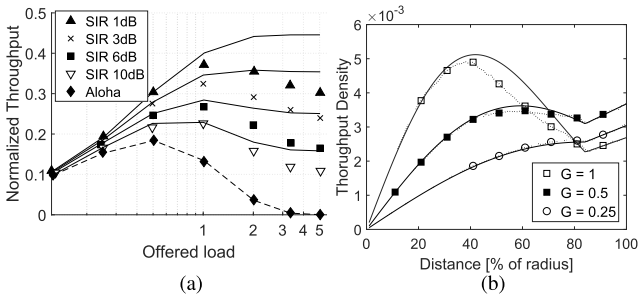

Fig. 5. Impact of single packet interference approximation on throughput with channel captures: theoretical model (solid lines) and simulation results including multiple packet interference (markers).

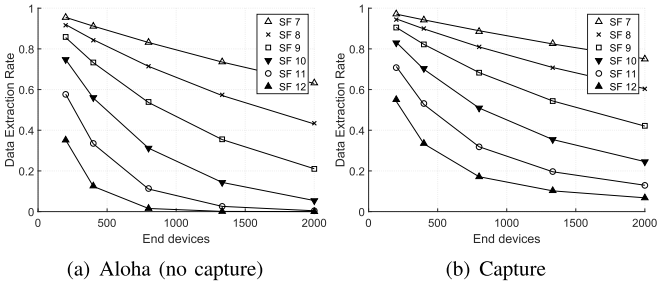

Fig. 6. Simulation (markers) and analytical model (lines) results for channel capture effect.

that all frames have fixed size with transmission time ToA_i, the throughput $S_c(G_i)$ in presence of captures obtained using SF i can be quantified by considering that the load offered in the circular ring between distance r and $r + dr$ will compete with the fraction $\min(\alpha^2 \cdot r^2/R^2, 1)$ of G_i:

$$S_c(G_i) = 2\pi \int_0^R \delta_i e^{-2\min(\frac{\alpha^2 r^2}{R^2},1)\cdot G_i} r \cdot dr \qquad (1)$$

where $\delta_i = G_i/(\pi R^2)$ is the density of load offered to SF i. It results:

$$S_c(G_i) = \frac{1}{2\alpha^2}\left(1 - e^{-2\cdot G_i}\right) + G_i\left(1 - \frac{1}{\alpha^2}\right)e^{-2\cdot G_i}$$

and the DER can then be obtained as $S_c(G_i)/G_i$.

In the previous derivation, we generically refer to a uniform load density δ_i, while in real cells we have a finite number n_i of EDs usually placed at fixed positions. However, we can generally consider that n_i is sufficiently high and the throughput derivation can refer to the average results obtained in different realizations of node placements.

Fig. 5-a shows the throughput curves obtained by equation 1 as a function of the offered load G_i, for several SIR values (i.e. α values). In the figure, the lines correspond to the analytical model (theoretical results), while the marker points represent the simulation results obtained with our Matlab simulator, in a simulation run of 9000 seconds. For deriving the average throughput results in simulation, we varied the offered load by adjusting the source rate of 1000 EDs and we randomly generated the position of each ED at each transmission attempt. The figure clearly shows that capture effects can significantly increase the maximum Aloha efficiency (up to about 300% for a capture SIR of 1dB when the offered load G_i is 1). Note that, our model works well in non-congested operating scenarios ($G_i < 1$), while it diverges from simulations in highly congested conditions, in which collisions involve multiple transmitted frames. Indeed, the asymptotic capacity of real systems tends to zero with the increase of the traffic load, while the model asymptotic value is different from zero (namely, it is equal to $1/2\alpha^2$).

To better visualize the effects of the load on the capacity approximation, Fig.5-b shows the throughput density (i.e. the integral argument in equation 1) achieved by EDs uniformly placed within the cell, as a function of the distance from the gateway (from 0 to 100% of the cell radius). Different curves refer to different G_i values: simulation results are shown with a dotted line and points, while our model results are plotted with solid lines. When the distance is higher than R/α and no capture effect is possible, we can easily recognize that the throughput density follows a linear distribution, because all EDs have the same success probability and the number of EDs considered in the integral grows proportionally to the distance. This last segments of the curve coincide with the throughput density of Aloha whose complete distribution is a linear distribution of the same slope in the whole interval $[0, R]$. For smaller distances, the capture effects can significantly increase the throughput density of Aloha. The figure also shows how our model overestimates the capture probability as the normalized load G_i increases: indeed, for $G_i = 0.25$ the points are perfectly overlapped with the solid line, while for $G_i = 1$ there is a region of the cell in which the real throughput is smaller than the one predicted.

Finally, we evaluated the DER achieved in a cell where all the nodes are configured on the same SF with and without the capture effects (for a capture SIR of 1 dB). Fig. 6 shows the DER results as a function of the number n of EDs configured on each SF, ignoring inter-SF interference. Each curve refers to an independent cell sub-system with the same number of EDs but different load conditions. The results demonstrate that the DER can increase significantly thanks to channel captures. For example for $n = 800$ EDs, using SF 10 the DER increases from about 0.32 in case of pure Aloha to about 0.52 in presence of captures. Obviously, for a fixed number of EDs n, lower SFs have the best DER because the resulting offered load is lower.

C. Impact of Imperfect Orthogonality

In order to quantify the impact of imperfect orthogonality among SFs on the cell capacity, we reasoned similarly to the previous section, by considering a single interfering signal at time. Because of imperfect orthogonality, a target ED working on SF i at a generic distance r will compete not only with the load G_i offered to the same SF, but also with a fraction of the load G_{-i} working with a SF different from i. Such a fraction corresponds to the EDs closer to the gateway, which generate an interfering signal whose power is much higher than the desired signal and exceeds the rejection capability of the LoRa receiver. Our experimental results showed that the SIR threshold under which interference rejection does not work is almost independent on the SF used by the interfering

signal. Therefore, the minimum required SIR value can be mapped into the placement of the interfering ED in a cell sub-region delimited by a radius $\beta_i \cdot r$, with $\beta_i = 10^{SIR/10\eta} < 1$, as shown in Fig. 4 (right).

The analysis of collisions between frames transmitted with different SFs requires taking into account that frames have heterogeneous transmission times, even if they have a fixed size P. Consider first a simple scenario in which channel captures with frames transmitted with the same SFs are not possible. In this case, interfering signals are given by the totality of transmissions performed with SF i and with the fraction $\beta_i r^2/R^2$ of transmissions performed with other SFs. The success probability of a target ED employing SF i depends on the probability of finding the channel free from other interfering signals when starting frame transmission and during the following time interval ToA_i. The probability Pr_s of finding the channel idle at the starting time of frame transmission is given by the probability that no packet arrival at SF i is originated within a previous interval lasting ToA_i, while a fraction $\beta_i r^2/R^2$ of other packets employing a different SF $k \neq i$ has not started a transmission in an interval corresponding to the relevant frame transmission time ToA_k. Such a probability can be expressed as:

$$Pr_s(r) = e^{-\lambda_i ToA_i - \frac{\beta_i r^2}{R^2}\sum_{k\neq i}\lambda_k ToA_k} = e^{-G_i} \cdot e^{-\frac{\beta_i r^2}{R^2} G_{-i}}$$

being $G_{-i} = \sum_{k\neq i} G_k$ the total load offered by SFs different from i. The probability Pr_e that no other interfering signal is started until the end of the transmission time ToA_i can be expressed as:

$$Pr_e(r) = e^{-(\lambda_i + \frac{\beta_i r^2}{R^2}\sum_{k\neq i}\lambda_k) ToA_i} = e^{-G_i} \cdot e^{-\frac{\beta_i r^2}{R^2} G^*_{-i}}$$

with $G^*_{-i} = \sum_{k\neq i}\lambda_k \cdot ToA_i = \lambda_{-i} ToA_i$. The total throughput obtained on sub-channel i with imperfect orthogonality between SFs can be computed by integrating the success probability experienced at each distance r over all possible distances as:

$$S_{qo}(G_i, G_{-i}) = 2\pi \int_0^R \delta_i Pr_s(r) \cdot Pr_e(r) r \cdot dr = \\ = e^{-2G_i} \cdot 2\pi \int_0^R \delta_i e^{-\frac{\beta_i^2 r^2}{R^2}(G_{-i} + G^*_{-i})} r \cdot dr \quad (2)$$

It results:

$$S_{qo}(G_i, G_{-i}) = G_i e^{-2\cdot G_i} \frac{1 - e^{-\beta_i^2 (G_{-i} + G^*_{-i})}}{\beta_i^2 \cdot (G_{-i} + G^*_{-i})} \quad (3)$$

which is obviously smaller than the ideal orthogonal case $S_o(G_i, G_{-i}) = G_i e^{-2\cdot G_i}$.

Finally, if we want to take into account both the capture effects and the imperfect orthogonality of SFs, we can follow the same approach discussed so far and specify that the competing load for each target ED working on SF i is the sum of a fraction $l = \min(\alpha^2\ r^2/R^2, 1)$ of the intra-SF load and a fraction $\beta_i^2\ r^2/R^2$ of the inter-SF load:

$$S_{qo,c}(G_i, G_{-i}) = 2\pi \int_0^R \delta_i e^{-\frac{\beta_i^2\ r^2}{R^2}(G_{-i} + G^*_{-i})} e^{-2\ lG_i} r \cdot dr$$

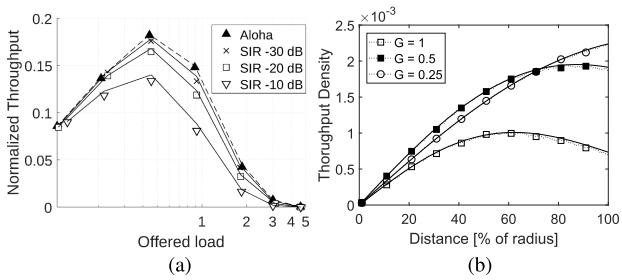

Fig. 7. Impact of single packet interference approximation on throughput with non orthogonal SFs: model approximation (lines) and simulation results including multiple packet interference (markers).

which leads to:

$$S_{qo,c}(G_i, G_{-i}) \\ = \frac{G_i e^{-2G_i}\left(1 - e^{-2G_i - (G_{-i} + G^*_{-i})\alpha^2/\beta_i^2}\right)}{2\alpha^2 G_i + \beta_i^2 (G_{-i} + G^*_{-i})} \\ + \frac{G_i e^{-2G_i}}{\beta_i^2 (G_{-i} + G^*_{-i})}\left(e^{(G_{-i} + G^*_{-i})\alpha^2/\beta_i^2} - e^{(G_{-i} + G^*_{-i})\beta_i^2}\right) \quad (4)$$

The average DER can then be computed by dividing the throughput with the total offered load.

To show the impact of inter-SF collisions, fig. 7-a shows the theoretical throughput curves (lines) obtained by equation 3 (no captures) for different values of the rejection SIR (i.e. β_i values), together with simulation results (points), when two different SFs coexist in the same cell (namely, SF 7 and SF 9). The curves refer to the throughput of EDs configured on SF 7. Also in this case, for deriving the average throughput results in simulation, we considered a fixed number of 1000 EDs (half configured on SF 7 and half on SF 9), varying the ED positions at each transmission attempt and tuning the source rate with increasing load. As shown in the figure, despite the pseudo-orthogonality of the SFs, the throughput can indeed be severely affected compared to the ideal Aloha without inter-SF collisions (almost 50% reduction in case of congested scenarios, i.e. $G_i \approx 1$). Fig. 7-b shows the throughput density (i.e. the integral argument in equation 2) achieved by EDs using 2 SFs with a rejection SIR of -10 dB and uniformly placed within the cell, as a function of the distance from the gateway (from 0 to 100% of the cell radius). Different curves refer to different G_i values: for low load conditions and small distances, the throughput density follows an almost linear distribution typical of Aloha with uniform EDs. However, for higher load conditions the curves can significantly deviate from a linear function, especially at high distances where inter-SF interference can be more critical.

Fig. 8 shows the DER results as a function of the total number N of EDs active in the cell, under the assumption that such a number is equally shared between different SFs (i.e. each SF is assigned to $n_i \approx N/6$ EDs) and same source rate s for all EDs. Again, markers represent simulations and lines the analytical results, which are still remarkably close to the simulations. From the figure, it is clear that the impact of

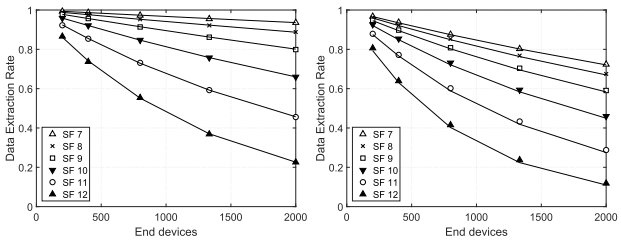

(a) Orthogonal SFs (b) Interfering SFs

Fig. 8. Simulation (markers) and analytical model (lines) results for interfering SFs.

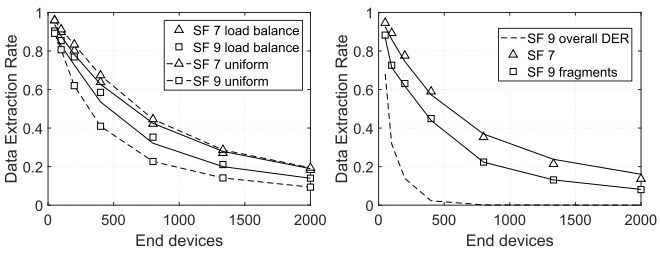

(a) Load balance (b) Fragmentation

Fig. 9. Impact of load balancing (left) and fragmentation (right) to increase fairness among the SFs.

non-orthogonality can be severe. The performance deteriorates quickly as the number of EDs increases.

V. Cell Configurations

In this section, we discuss the impact of different cell configurations that can be considered for optimizing the cell capacity when multiple SFs are available. For sake of presentation, we consider two SFs only, namely SF i < SF j, but generalizations to multiple SFs are straightforward. From our previous considerations, it is evident that LoRa cell performance is a function of the arrival rates of packets working on SF i and SF j, but also of their placement within the cell, because the inter-SF and intra-SF interference power experienced in case of collisions also depends on the relative position of the EDs.

A. Load Balancing

Assuming that a total arrival rate of Λ pk/s is uniformly distributed within the cell, the arrival rates λ_i and λ_j experienced in each SF (with $\lambda_i+\lambda_j = \Lambda$) depend on the SF selected for each packet transmission. The selection of the certain SF may be a local decision, such as the selection of the highest possible rate compatible with the link budget available at a given spatial position, or may be extended with load balancing considerations. If the link budget at the cell border is enough for transmitting at the highest rate corresponding to SF i, the first approach would lead to $\lambda_i = \Lambda$ and $\lambda_j = 0$. Load balancing can significantly improve the overall cell capacity by reducing the load on SF i and by exploiting the additional capacity available on SF j.

A balancing solution devised to provide fair performance to devices working on different SFs is equalizing the offered load $G_i = G_j$. Note that this is different from equalizing the number of transmissions performed at each SF, because packet transmission times vary as a function of the employed SF. Specifically, load balancing is achieved for $\lambda_i \cdot ToA_i = \lambda_j \cdot ToA_j$, i.e. $\lambda_i = \Lambda \cdot \frac{ToA_j}{ToA_j+ToA_i}$. This implies that in a real cell with a finite number N of EDs, if all EDs work with uniform source rates, the same proportion is applied for deriving n_i as $N \cdot \frac{ToA_j}{ToA_j+ToA_i}$. However, perfect load balancing is not always feasible, because some EDs distant from the gateway can be forced to work on the most robust SF for guaranteeing that the received power is above the reception threshold.

Fig. 9-a compares the DER obtained in a cell with a total number N of EDs and two SFs available (namely, SF 7 and SF 9). Simulation results are shown with markers and model results with lines. The figure shows results for different criteria on SF allocations: equally sharing the number of EDs between SF 7 and SF 9 (dashed lines) or allocating a number of EDs proportionally to the relevant airtimes, with n_7 about four times of n_9 (solid lines). From the figure, it is evident that the second choice, i.e. load balancing, can be an effective solution for providing a similar DER to all devices, regardless of the allocated SF. However, DER performance are not exactly the same because inter-SF interference is not symmetrical due to different rejection thresholds (i.e. β_i and β_j coefficients) and transmission times (which result in $G^*_{-i} < G^*_{-j}$ even in case of load balancing). Overall, the most robust SF j suffers an higher inter-SF competing load.

An additional mechanism to be considered for improving the fairness of the system could be the use of fragmentation. The idea is to equalize the airtimes of packets transmitted at different SFs. Obviously, in such a case, the arrival rates of fragments grow proportionally to the number of per-packet fragments. Fig. 9-b shows the performance results in the same scenario described for Fig. 9-a, with n_7 about four times n_9, and 4 fragments are used for packets transmitted with SF 9. From the figure, it is clear that fragmentation is not effective for equalizing the performance of the EDs, due to the additional overhead added to each fragment. Additionally, we have to consider that now four fragments are required for reassembling a single packet at SF 9. Thus, the overall DER (dashed line) is worse than the previous case. This is also due to the fact that LoRa technology does not easily support selective re-transmissions of corrupted fragments, because the downlink channel from the gateway to the EDs would result congested by the transmission of the feedback messages. Therefore, fragmentation without selective re-transmissions does not bring benefits to the network.

B. Spatial Allocations

For a fixed number of EDs n_i (or n_j) to be configured on SF i (or SF j), different allocation choices are possible. EDs working on the same SF can be selected uniformly within the whole cell area or can be restricted to a specific area of the cell. According to the position of the selected nodes, each allocation policy can be mapped into the opportunistic

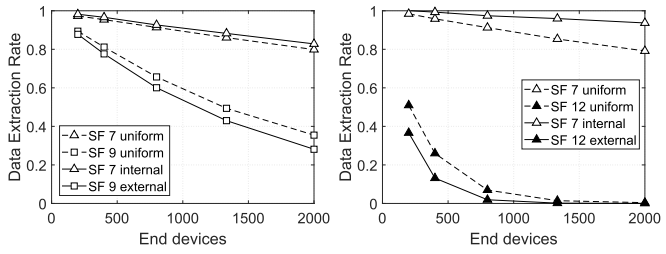

Fig. 10. Performance of SF9 (a) and SF12 (b) when competing with SF7. Comparison between uniform distribution of EDs (dashed lines) and when higher SFs are allocated to far away EDs (solid lines). The inter-SF SIR threshold is 10 dB and $\eta = 4$.

definitions of the $\delta_i(r)$ and $\delta_j(r)$ functions. In order to predict the cell capacity resulting from a specific allocation, we can generalize previous throughput derivations for dealing with non uniform load density functions.

As an illustrative example of model extension under generic $\delta_i(r)$ functions, we consider the case in which nodes employing different SFs are placed in different sub-regions of the cell, rather than being uniformly spread in the whole area. A choice could be allocating the most robust SF to far users, placed in a circular ring between distance $d > 0$ and R, and the less robust SF to users closer to the gateway within a maximum distance d, in order to maximize the reception margin of each ED. The distance d can be chosen for achieving the desired load balancing. In such a case, the density functions of nodes employing different SFs can be defined as: $\delta_i(r) = G_i/(\pi d^2)$ when $r \leq d$ (and 0 otherwise), and $\delta_j(r) = G_j/(\pi R^2 - \pi d^2)$ when $r < d$, and 0 otherwise.

Allocating EDs in circular rings have different implications for both the inter-SF and the intra-SF interference. Regarding the first aspect, by neglecting the fading effects, it never happens that users employing spreading factor SF i are interfered by users employing SF j with a higher interfering power (being these users deterministically located at higher distances). In other words, the throughput achieved on spreading factor SF i is given by $S_i = G_i \cdot e^{-2 \cdot G_i}$, i.e. the density of potentially interfering signals is equal to zero as in case of perfect orthogonality. Conversely, users employing spreading factor SF j are more likely affected by interference generated by users employing spreading factor SF i, because in case of collisions the interfering signals are concentrated in the cell area closer to the gateway, which results in a interference density higher than the previous case. Being $\delta_{-i}(r) = \sum_{j \neq i} \delta_j(r)$ and $\delta^*_{-i}(r) = \sum_{j \neq i} \delta_j(r) \frac{ToA_i}{ToA_j}$, the throughput in absence of channel captures becomes:

$$S_{qo}(i) = e^{-2\pi \int_0^R 2\delta_i(r) r \cdot dr} \cdot \cdot 2\pi \int_0^R \delta_i(r) \left[e^{-2\pi \int_0^{\beta_i r} (\delta_{-i}(t) + \delta^*_{-i}(t)) t \cdot dt} \right] r \cdot dr \quad (5)$$

Figures 10-a and 10-b compare the performance of SF 7 when competing with SF 9 and SF 12 respectively, in scenarios with uniform allocation of SFs in the cell (dashed lines) or when far distance EDs are using the highest SF 9 and SF 12, while SF 7 is used for EDs close to the gateway. The figures show that the performance of the higher SFs is deteriorated when allocating them to faraway EDs, while SF 7 performance improves because of the absence of inter-SF collisions. This, demonstrates that allocating higher SFs to far distance EDs is detrimental more than beneficial, because the performances are highly affected by closer devices while fading has a much lower impact. In other words, although higher SFs improve the robustness to fading and allow longer distances, this comes at the cost of an increased airtime of the transmitted frames and, since LoRa uses the Aloha access protocol, collisions arise quickly when increasing the offered load. Clearly, using low SFs for long distances might cause unnecessary retries, or even no packet delivery at all in case the link budget is not sufficient.

SF allocation has also an impact on the capture probability. For a given number n_i of EDs working on SF i, the highest capture probability is achieved when nodes are spread in the whole cell (rather than in a circular ring), because this choice corresponds to the spreading of the RSSI values of potentially colliding signals (which may result in the correct reception of the strongest signal). In the limit case in which all nodes working on SF i are at the same distance from the gateway, no capture effect can occur.

C. Power Control

Another important configuration parameter of LoRa cells is the transmission power of EDs, which can be tuned by means of specific control messages sent by the gateway. The message specifies the power to be used in terms of a reduction margin to be applied to the maximum possible power (which may vary in different countries); the reduction margin is coded in steps of -2dB from 0 to -14dB. The tuning of the transmission power can be considered for reducing the energy consumption of devices which are close to the gateway, but also for mitigating the impact of inter-SF interference, Indeed, orthogonality of different SFs can be guaranteed in case the difference between the reception powers of EDs working at different SFs is lower than the minimum margin in table I (about -8dB).

To model the impact of power control on the LoRa cell performance, we can consider that each power reduction applied to a specific ED is equivalent to moving the device at an higher distance from the gateway. If η is the propagation loss coefficient, every step of -2dB corresponds to a distance increment of a factor equal to $\gamma = 10^{2/10\eta}$. In case power control is used for equalizing the reception power of the EDs, taking into account that only -14dB are available at steps of -2dB and the distance r_{min} of the closer ED, we could equivalently consider that no ED is placed at a distance lower than $d = 10^{14/10\eta} \cdot r_{min}$ and that EDs originally placed within the circular area of radius d are moved in the circular ring between d and $d \cdot \gamma$. In other words, power control can be evaluated again by working on the definition of the load density function $\delta_i(r)$ as follows: 0 when $r < d$, $G_i/(\pi R^2) \cdot [1 + 1/(\gamma^2 - 1)]$ when $r \in [d, d \cdot \gamma]$, and $G_i/\pi R^2$ when $r > d \cdot \gamma$. Equivalently, we can define $\delta_j(r)$ and derive the cell capacity S_{qo} of each SF applying equation 5.

As an illustrative example, we consider a cell using only SF 7 and SF 9, with half of the EDs using SF 7 are placed

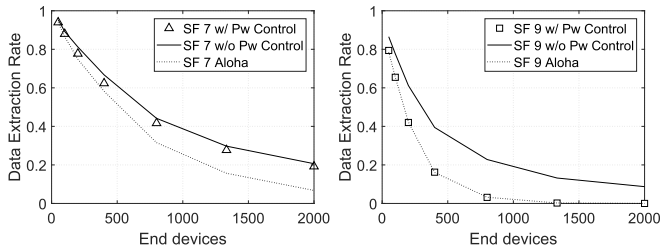

(a) SF7 (b) SF9

Fig. 11. DER with two interfering SFs with and without using transmission power control.

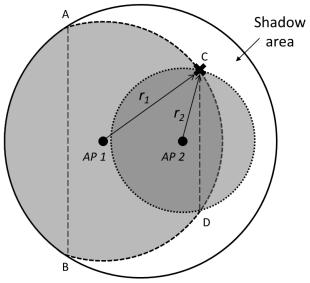

Fig. 12. Competing area (gray) in presence of multiple gateways and "shadow area" created by the ED in position C.

close to the gateway and the others using SF 9 are far away from the gateway. For clearness of presentation, Fig. 11 reports separately in two plots the DER achieved by the two SFs, although in the experiment both SFs are used as explained above. From the figure, it is evident that when equalizing the received power, the DER of SF 9 is close to the Aloha model (no channel captures) and much lower than the DER obtained without power control, while for SF 7 there is almost no change. This means that tuning the transmitted power of the EDs in order to equalize the received power at the gateway is detrimental more than beneficial for performance because, in case of collision between packets of the same SF, it reduces the probability of capturing the channel.

VI. Cell Capacity With Multiple Gateways

Thanks to the capture effect, the capacity of a LoRa cell can be increased by deploying multiple gateways. Indeed, each gateway sees a given ED with a different distance and therefore, in case of collisions, experiences a different power ratio between the strongest received packet and the interfering signals. When the power ratios are higher than the capture threshold, the collisions can result in the correct reception of a number of packets equal at most to the number of gateways. Obviously, it may also happen that the same packet is correctly received by multiple gateways, but all the packets are forwarded to a common network server, which discards duplicated packets.

For deriving the average cell capacity in presence of multiple gateways, it is necessary to specify the positions of the gateways within the cell, because the capture probability depends on the relative distance between the potential receivers (i.e. the gateways) and the transmitters. Differently from the single gateway case, even under the assumption that only a colliding signal is experienced at a given time, the EDs competing with a target transmitter are different for each gateway and distributed in regions which cannot be modeled as simple circle areas. For example, Fig. 12 shows the scenario of a cell with two gateways, $\alpha = 1$ and uniform distribution of EDs: the target transmitter in position C experiences different competing loads at each gateway, which are proportional to the intersection area between a circle of radius αr_m and the cell, being r_m the distance between the ED and a generic gateway $m = 1, 2$. Although the areas can be computed as circular areas delimited by the chords AB and CD, it is not easy to generalize the approach proposed in §IV, because the performance of the target transmitter cannot be averaged as a function of the distance from the cell center, being also affected by the direction (i.e. by the specific position within the cell).

For a specific placement of the gateways, we modeled the geometry of the cell under uniform distribution of the EDs and complete coverage (i.e. assuming that EDs can transmit to a gateway placed at distance $2 \cdot R$) by numerically evaluating the average probability γ_k that a target ED successfully transmits its packet to at least one gateway, in presence of $k \geq 0$ interfering EDs. By considering one interfering signal at time as in the single gateway derivation, such a probability has been computed by averaging (on all possible transmitter positions) the probability that, for at least one gateway, k interfering EDs are at distances higher than α times the distance of the target transmitter. The analysis of the capture probability in presence of k interfering EDs allows us the decoupling between the geometric effects (due to the specific gateway placement) and the interference probability (due to the cell load). In other words, assuming that the γ_k coefficients are known, the cell capacity in presence of multiple gateways can be computed for any possible load G_i as:

$$S_c(i) = G_i \cdot \left[\sum_{k=0}^{\infty} \left(\gamma_k \frac{(2G_i)^k \, e^{-2G_i}}{k!} \right) \right]. \qquad (6)$$

Note that, when $SIR = 0$ dB (i.e. $\alpha = 1$) and a single gateway is placed in the center of the cell, then $\gamma_k = 1/(k+1)$, because for any placement of $k+1$ EDs, only one ED will result closer to the single gateway (assuming negligible the probability of extracting two EDs on the same distance to the gateway). In this condition, it is easy to see that equation (6) gives the same result of equation (1).

Obviously, the γ_k coefficients depend not only on the number of gateways but also on their specific position within the cell. Since a closed form derivation is not generally possible, we evaluated the γ_k coefficients numerically for specific gateway positions. To this purpose, we randomly generated $k+1$ EDs uniformly distributed in the cell, quantified the ratio of EDs whose distance r from at least one gateway was α times smaller than the distance between the other k EDs and the same gateway, and averaged results over multiple random placements. In our evaluations, we analyzed different deployment strategies: placing the gateways at a regular grid,

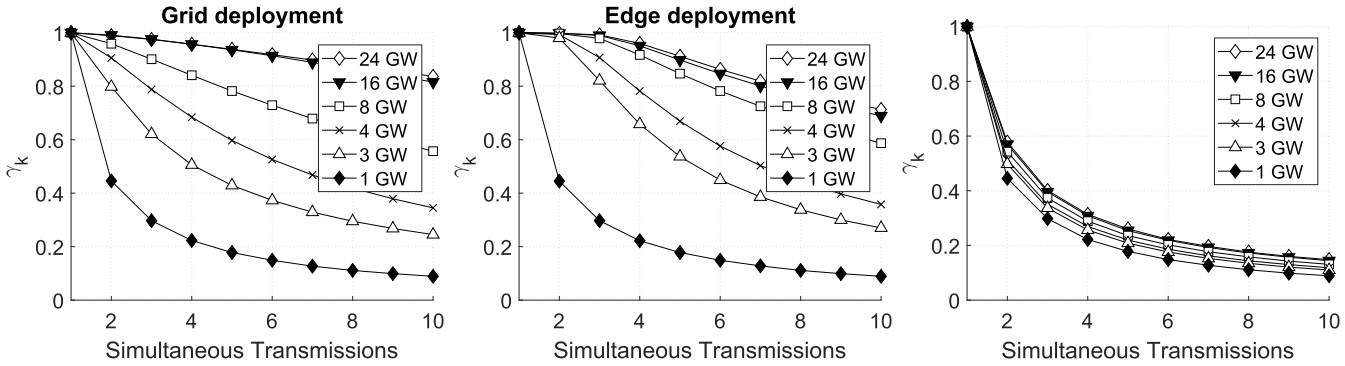

(a) Grid (b) Edge (c) Center

Fig. 13. Impact of gateway deployment: values of γ_k with $\eta = 4$, SIR= 1dB and different number of gateways on a grid deployment (a), at the cell edge (b), or when the gateways are all concentrated close to the center of the cell(c).

on the cell edge, or concentrated very close to the cell center. For the grid deployments, we kept a central symmetry towards the cell center, by equally spacing the gateways in the two cell dimensions; for the edge deployment, we equally spaced the gateways along the cell circumference, while for the last setting we created a small grid of size $R/10$.

A. Capture Probability

Fig. 13 shows the γ_k results numerically obtained by placing a varying number of gateways with the three deployment strategies explained above: from the figure, it is easy to see how γ_k coefficients are strongly dependent on the gateway placements. This is particularly evident in the last case: when the gateways are too close to each other, the performance does not improve in comparison with the single gateway cell. Indeed, the space diversity between gateways is poor and offers little opportunities for increasing the channel captures. For the other deployment solutions, we also observe that coefficients result generally higher when the gateways are placed on the cell edge rather than on a regular grid. Only when the number of gateways is high (e.g. 16 or 24) the grid topology is better, although the improvement on the capture probability is marginal. Although not intuitive, this result can be justified by considering that (as long as coverage is guaranteed) the more the gateways are sparse, the more channel captures can be achieved. For example, for $k = 1$ (one interferer, 2 simultaneous transmissions) and 3 gateways, the average number of transmissions correctly received by at least one gateway is 0.999 for gateways deployed on the cell edge and 0.804 for gateways placed in a regular grid. As depicted in Fig. 12, on a grid topology a transmitting ED can create a "shadow area" towards the cell edge, impeding any other ED in this area to successfully capture the channel.

B. Throughput:

Fig. 14 quantifies the cell throughput by using equation 6 and the γ_k coefficients derived in our numerical evaluations, for the grid (solide lines) and edge (dashed lines) deployment strategies. The figures clearly show that increasing the number of gateways allows to achieve a throughput almost equal to

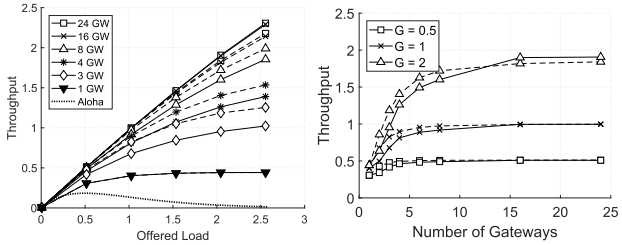

(a) (b)

Fig. 14. Grid deployment (solid) vs. edge deployment (dashed) when varying the offered load or the number of gateways.

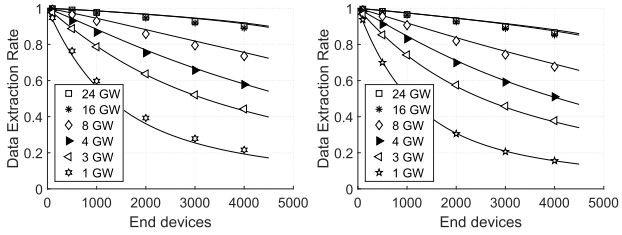

(a) SIR=1dB. (b) SIR=3dB.

Fig. 15. DER using multiple gateways in a grid topology: model (lines) and simulation results (points) for SIR values of 1 and 3 dB.

the offered load. Obviously, higher capture probabilities are mapped into higher throughput results. For example, with 3 gateways the throughput achieved with the edge deployment is about 25% higher than the one achieved with the regular grid, while for a number of gateways equal or higher than 16 the throughput gain of the grid deployment is about 5%. We can expect that these capacity differences under different gateway deployments can be reduced in case of multi-cell systems.

In order to validate our model, Fig. 15 compares our throughput predictions with simulation results. For space reason, we only show results for the regular grid case (but conclusions are similar for the edge deployment case). The figures have been obtained by considering the availability of one SF only (namely, SF7) and three different capture thresholds (0, 1 and 3 dB). The figure allows to draw some

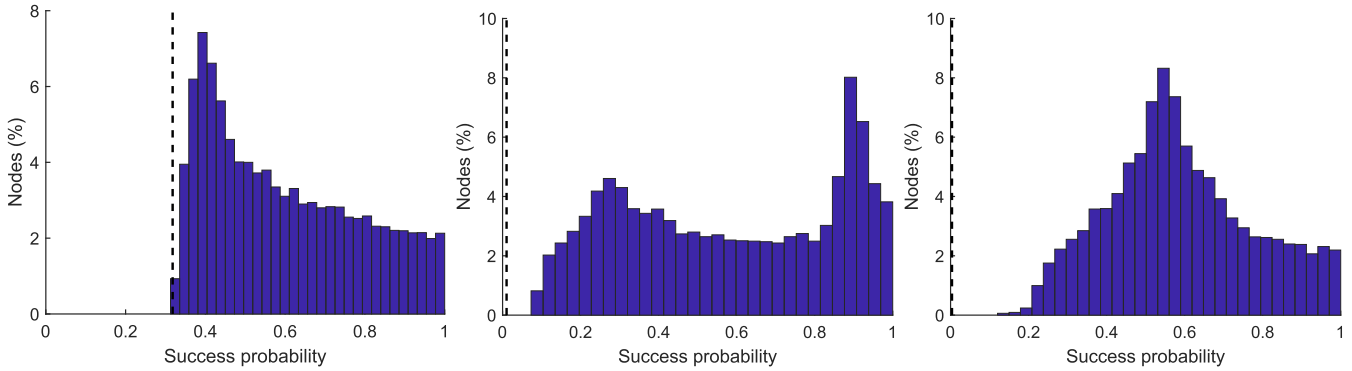

(a) 1 GW Center (b) 4 GW Grid (c) 4 GW Edge

Fig. 16. Impact of gateway deployment on fairness: distribution of the success probability among EDs in a cell with 1 gateway in the center (a) and with 4 gateways in a regular grid (b) or at the cell edge (c).

interesting conclusions. First, despite of the simplification assumptions used for modeling the capture effects, the model is in agreement with simulations in all the considered scenarios, thus validating equation 6 and the γ_k derivation. Second, when the capture effects are very common (i.e. for capture threshold of 0 dB), a cell with M gateways and a number of devices equal to N provides similar performance of M independent systems loaded with N/M devices. For example, the DER achieved with 4 gateways and 2000 EDs results slightly less than 0.8 and comparable with the one achieved by a single gateway with 500 EDs or 8 gateways and 4000 EDs. Third, the capture threshold has a much lower impact than in a single gateway case, thanks to the increased capture possibilities provided by the spatial diversity of the gateways. Finally, although results always improve as the number of gateways increases, at a given point the improvements are marginal (DER results with 16 or 24 gateways are almost comparable).

C. Fairness

The position of the gateways has also a significant impact not only on the average cell performance, but also on the fairness of the network, i.e. on the spreading of the DER results achieved by different EDs. Fig. 16 shows the success probability histogram of the ED's transmissions in various scenarios characterized by *same* DER of 0.6 but different number of gateways, EDs and deployment strategy. In particular, the figure shows what happens in a cell with 1 gateway in the center or with 4 gateways, in a regular grid or at the cell edge. To obtain the same DER of 0.6, the number of EDs was 1000, 4000 and 4900 respectively and the corresponding offered load was 0.57, 2.29 and 2.81 (these values were obtained experimentally to equalize the capacity and achieve equal DER for all scenarios). From the figure, it is clear that with only one gateway most of the EDs have low performances, while in a grid topology the distribution is bimodal, with a group of EDs that transmit with very high success probability (higher than 80%) and another group which suffer low performance (around 30% successful frames). Instead, the edge deployment tends to be more fair, in the sense that most of the EDs experience a success probability around 0.6, corresponding to the cell average DER. The figure also shows the minimum theoretical success probability of the pure Aloha system (given by e^{-2G} and marked by the dashed lines), which is obviously different for the three scenarios because of the different load levels. Note that the capture effects can improve the Aloha results for some devices, without penalizing the ones with low capture probabilities.

VII. Conclusion

In this paper we have studied the impact of two peculiar characteristics of LoRa modulations, i.e. the high capture probability and the imperfect orthogonality between different SFs, on the overall cell capacity. Although parallel reception of multiple overlapping frames is generally possible, we showed that the link-level performance of LoRa is deeply influenced by capture effects and by inter-SF collisions which can indeed cause loss if the interference power is strong enough.

We then exploited this link-level analysis to model analytically the achievable network capacity in a typical LoRa cell. We showed that high SFs are severely affected by inter-SF interference and that the use of power control and packet fragmentation to compensate such problem may be counterproductive. Although deploying multiple gateways can mitigate the capacity loss and boost the occurrence of channel captures, the overall capacity increase becomes negligible after 16-24 gateways. Finally, when only a handful of gateways are present, the deployment should be as distant from the center as possible and not on a regular grid.

We believe that the results presented in this paper provide important insights on LoRa technology and can pave the way to new accurate guidelines for the correct design of future LoRa networks.

References

[1] *Worldwide Connected Devices Forecast*. Accessed: Oct. 23, 2019. [Online]. Available: www.statista.com

[2] Semtech. *Lora Modulation Basics AN1200.22*. Accessed: May 2, 2015. [Online]. Available: www.semtech.com

[3] M. C. Bor, U. Roedig, T. Voigt, and J. M. Alonso, "Do LoRa low-power wide-area networks scale?" in *Proc. MSWiM*. New York, NY, USA: ACM, 2016, pp. 59–67.

[4] B. Reynders and S. Pollin, "Chirp spread spectrum as a modulation technique for long range communication," in *Proc. SCVT*, Mons, Belgium, 2016, pp. 1–5.
[5] B. Reynders, W. Meert, and S. Pollin, "Range and coexistence analysis of long range unlicensed communication," in *Proc. ICT*, Thessaloniki, Greece, 2016, pp. 1–6.
[6] D. Croce, M. Gucciardo, S. Mangione, G. Santaromita, and I. Tinnirello, "Impact of LoRa imperfect orthogonality: Analysis of link-level performance," *IEEE Commun. Lett.*, vol. 22, no. 4, pp. 796–799, Apr. 2018.
[7] M. Gucciardo, I. Tinnirello, and D. Garlisi, "Demo: A cell-level traffic generator for LoRa networks," in *Proc. 23rd Conf. Mobile Comput. Netw. (MobiCom)*, Snowbird, UT, USA, Oct. 2017, pp. 474–476.
[8] C. Goursaud and J. M. Gorce, "Dedicated networks for IoT: PHY / MAC state of the art and challenges," *EAI Endorsed Trans. Internet Things*, vol. 1, Oct. 2015, Art. no. 150597.
[9] *LoRaSim*. Accessed: Oct. 23, 2019. [Online]. Available: https://www.lancaster.ac.uk/scc/sites/lora/lorasim.html
[10] L. Vangelista, A. Zanella, and M. Zorzi, "Long-range IoT technologies: The dawn of LoRa," in *Future Access Enablers of Ubiquitous and Intelligent Infrastructures* (Lecture Notes of the Institute for Computer Sciences, Social Informatics and Telecommunications Engineering), vol. 159. Cham, Switzerland: Springer, 2015, pp. 51–58.
[11] A. Augustin, J. Yi, T. Clausen, and W. M. Townsley, "A study of LoRa: Long range & low power networks for the Internet of Things," *Senors*, vol. 16, no. 9, p. 1466, 2016.
[12] M. Knight and B. Seeber, "Decoding LoRa: Realizing a modern LPWAN with SDR," in *Proc. GNU Radio Conf.*, Sep. 2016, vol. 1, no. 1, pp. 1–5.
[13] D. Bankov, E. Khorov, and A. Lyakhov, "On the limits of LoRaWAN channel access," in *Proc. Int. Conf. Eng. Telecommun. (EnT)*, Moscow, Russia, Nov. 2016, pp. 10–14.
[14] F. Cuomo, M. Campo, A. Caponi, G. Bianchi, G. Rossini, and P. Pisani, "Explora: Extending the performance of lora by suitable spreading factor allocations," in *Proc. IEEE 13th Int. Conf. Wireless Mobile Comput., Netw. Commun. (WiMob)*, Oct. 2017, pp. 1–8.
[15] K. Q. Abdelfadeel, V. Cionca, and D. Pesch, "Fair adaptive data rate allocation and power control in Lorawan," in *Proc. IEEE 19th Int. Symp. A World Wireless, Mobile Multimedia Netw. (WoWMoM)*, Jun. 2018, pp. 14–15.
[16] B. Reynders, W. Meert, and S. Pollin, "Power and spreading factor control in low power wide area networks," in *Proc. IEEE Int. Conf. Commun. (ICC)*, May 2017, pp. 1–6.
[17] M. Zorzi and R. R. Rao, "Capture and retransmission control in mobile radio," *IEEE J. Sel. Areas Commun.*, vol. 12, no. 8, pp. 1289–1298, Oct. 1994.
[18] D. J. Goodman and A. A. M. Saleh, "The near/far effect in local ALOHA radio communications," *IEEE Trans. Veh. Technol.*, vol. VT-36, no. 1, pp. 19–27, Feb. 1987.
[19] *LoRaWAN Regional Parameters v1.1rB*. Accessed: Oct. 23, 2019. [Online]. Available: https://lora-alliance.org/resource-hub/lorawanr-regional-parameters-v11rb
[20] Le T. Tan and L. B. Le, "Distributed MAC Protocol design for full-duplex cognitive radio networks," in *Proc. IEEE Global Commun. Conf. (GLOBECOM)*, San Diego, CA, USA, Dec. 2015, pp. 1–6.
[21] Le T. Tan and L. B. Le, "Multi-channel MAC protocol for full-duplex cognitive radio networks with optimized access control and load balancing," in *Proc. IEEE Int. Conf. Commun. (ICC)*, Kuala Lumpur, Malaysia, May 2016, pp. 1–6.

Daniele Croce received the Ph.D. degree jointly from the Politecnico di Torino, Turin, Italy, and the Université de Nice-Sophia Antipolis (UNSA), Nice, France, in 2010, and the double M.Sc. degree in networking engineering from the Politecnico di Torino and EURECOM Institute, Sophia Antipolis, France, in 2006, and the Research Master Diploma degree (ex DEA) in networking and distributed systems from UNSA, France.

He currently holds a research position at the Sapienza University of Rome. He has long experience of research collaborations, in several European and national research projects, on wireless networks, the Internet of Things, high-quality TV streaming, smart grid communications, and smart cities. He also worked on assistive technologies for visually impaired people and with the Arianna project and he co-founded the start-up company In.sight s.r.l., spin-off of Palermo University, Italy.

Michele Gucciardo received the B.Sc. degree from Politecnico di Milano, Italy, in 2008, and the M.Sc. degree from the University of Palermo, Italy, in 2013, all in telecommunications engineering. He is currently pursuing the Ph.D. degree in information and communication technologies with the University of Palermo.

He has also been a Visiting Researcher at the TIM Labs, Turin, Italy, and at the IMDEA Networks Institute, Madrid, Spain, in 2018 and 2019. His research interests have been focused on the experimental evaluation of emerging the IoT technologies, software defined infrastructures and machine learning in 5G, and computational offloading in wireless networks.

Stefano Mangione received the degree *(cum laude)* in electronics engineering and telecommunications curriculum in 2000.

He is currently an Assistant Professor in telecommunications engineering with the University of Palermo. His research activities have been focused on physical-layer aspects of communication systems, from forward error correction coding to equalization strategies for spread spectrum systems. Recently, his activities include automatic methods for registration of nuclear magnetic resonance images, multiuser receiver strategies for LoRa, and the study of underwater communication systems.

Giuseppe Santaromita received the bachelor's degree in information and telecommunications engineering and the master's degree in telecommunications engineering from the University of Palermo in 2014 and 2016, respectively, where he is currently pursuing the Ph.D. degree in information and communication technologies.

He has also been a Visiting Researcher at the IMDEA Networks Institute, Spain, in 2019. His research activities have been focused on wireless networks, and in particular on the programmable PHY layer for optimizing wireless networks performance.

Ilenia Tinnirello received the Ph.D. degree in telecommunications engineering from the University of Palermo in 2004. She is currently an Associate Professor with the University of Palermo. She has also been a Visiting Researcher at Seoul National University, South Korea, in 2004, and at the Nanyang Technological University of Singapore in 2006. Her research activities have been focused on wireless networks and in particular on the design and prototyping of protocols and architectures for emerging reconfigurable wireless networks. Recently, she is also working on the definition of novel services (smart grid, smart metering, and indoor localization) enabled by the pervasive availability of ICT technologies. She has been involved in several European research projects, among which the FP7 FLAVIA project, with the role of Technical Coordinator, and the H2020 WiSHFUL and Flex5Gware projects.